

## TIME-DOMAIN INVERSE SCATTERING OF A TWO-DIMENSIONAL METALLIC CYLINDER IN SLAB MEDIUM USING ASYNCHRONOUS PARTICLE SWARM OPTIMIZATION

C.-H. Sun, C.-C. Chiu, and C.-L. Li

Electrical Engineering Department  
Tamkang University  
Tamsui, Taipei, Taiwan, R.O.C.

**Abstract**—This paper presents asynchronous particle swarm optimization (APSO) applied to the time-domain inverse scattering problems of two-dimensional metallic cylinder buried in slab medium. For this study the finite-difference time-domain (FDTD) is employed for the analysis of the forward scattering part, while for the APSO is applied for the reconstruction of the two-dimensional metallic cylinder buried in slab medium, which includes of the location and shape the metallic cylinder. For the forward scattering, conceptually several electromagnetic pulses are launched to illuminate the unknown scatterers, and then the scattered electromagnetic fields around are measured. In order to efficiently describe the details of the cylinder shape, sub-gridding technique is implemented in the finite difference time domain method. Then, the simulated EM fields are used for inverse scattering, in which APSO is employed to transform the inverse scattering problem into optimization problem. By comparing the simulated scattered fields and the calculated scattered fields, the shape and location of the metallic cylinder are reconstructed. In addition, the effects of Gaussian noises on imaging reconstruction are also investigated.

### 1. INTRODUCTION

The detection and reconstruction of buried and inaccessible scatterers by inverting microwave electromagnetic measurements is a research field of considerable interest because of numerous applications in civil

engineering and nondestructive testing. Numerical inverse scattering studies found in the literature are based on either frequency or time domain approaches. With frequency domain algorithms, the interaction of the entire medium with the incident field is considered simultaneously. In contrast, time-domain approaches can exploit causality to limit the region of inversion, potentially reducing the number of unknowns. Time domain inverse scattering problems somewhat related to the present study commonly appear in the area of remote sensing. However, it is well known that one major difficulty of inverse scattering is its ill-posedness and non-unique in the inverse scattering problems [1, 2].

In the past twenty years, the inversion techniques are developed intensively for the microwave imaging both in frequency domain and time domain [3–16]. Most of the inversion techniques are investigated for the inverse problem using only single frequency scattering data (monochromatic source) [3–5]. However, the time domain scattering data is important for the inverse problem because the available information content about scatterer is more than the only single frequency scattering data. Finite-difference time-domain (FDTD) method has advantage that compared with frequency domain. FDTD method provides the capability to model arbitrary metallic objects and lossy homogeneous backgrounds. Moreover, multiple frequencies can be investigated without any extra computational effort. Therefore, various time domain inversion approaches are proposed [6–11] that could be briefly classified as the neural networks [6], the iterative approach: Born iterative method (BIM) [7], and gradient-based method [8], and optimization approach [9–11]. Traditional iterative inverse algorithms are founded on a functional minimization via some gradient-type scheme. In general, during the search of the global minimum, they tend to get trapped in local minima when the initial guess is far from the exact one. Asynchronous particle swarm optimization (APSO) [12] is well-known evolutionary algorithm of optimization strategy, which uses stochastic mechanism to search through the parameter space. In recent year, most of the researchers have applied APSO together with the frequency domain EM solver for the inverse problems [13]. Fewer researchers had applied the genetic/evolutionary algorithms in time domain for the inverse scattering problem for target identification [14, 15] and penetrable object reconstruction [16]. To the best of our knowledge, a comparative study about the performances of particle swarm optimization (PSO) and asynchronous particle swarm optimization (APSO) has not yet been reported with application to the electromagnetic inverse scattering problems.

This paper presents a time domain computational scheme for the microwave imaging of a 2D metallic cylinder with arbitrary shape buried in the subsurface. The computational method combines the FDTD method and the APSO [12]. The forward problem is solved based on the FDTD method, for which the subgridding technique is implemented to closely describe the fine structure of the cylinder [17,18]. Interpolation technique through the closed cubic B-splines [19] is employed to describe a cylinder with arbitrary shape more effectively. In Section 2, the details of the subgridding FDTD method for the forward scattering are presented. In Section 3, the numerical results of the proposed inverse problem are given. The shadowing effect is shown, and the techniques proposed to overcome it are demonstrated. Finally, in Section 4 some conclusions are drawn for the proposed time domain inverse scattering.

## 2. FORWARD PROBLEM

Let us consider a two-dimensional three-layer structure with buried conducting cylinder in the second layer as shown in Fig. 1, where  $(\epsilon_i, \sigma_i)$   $i = 1, 2, 3$ , denote the permittivities and conductivities in each layer. The metallic cylinder with cross section described by the equation  $\rho = F(\theta)$  is illuminated by an incident plane wave whose electric field vector is parallel to the  $z$  axis. The cross section of the

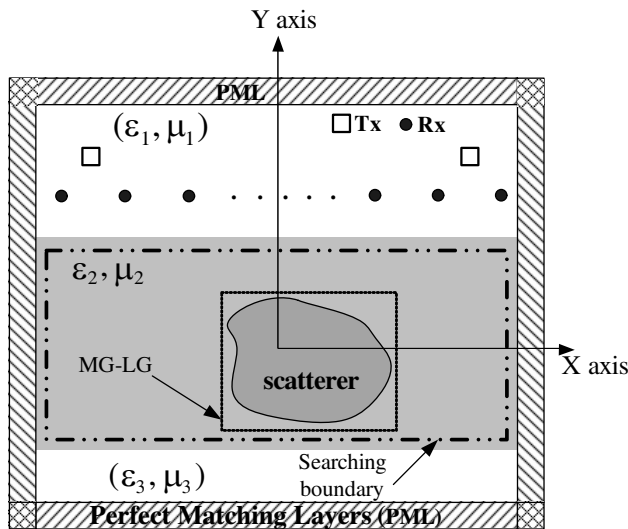


Figure 1. Geometrical configuration for the inverse scattering.

object is starlike shape in the  $x$ - $y$  plane with respect to the center position  $(X_O, Y_O)$ . The metallic cylinder is illuminated by Gaussian pulse line source located at the points denoted by Tx in the first layer. Scattered waves are recorded at those points denoted by Rx in the same layer. The computational domain is discretized by Yee cells. It should be mentioned that the computational domain is surrounded by the optimized perfect matching layers (PML) absorber [20] to reduce the reflection from the environment-PML interface.

The  $E$  field data need to be obtained in the forward scattering problem by the FDTD code with fine grids to mimic the experimental measurement data. For the forward scattering problem the shape and location of the metallic cylinder to be determined is given first, and then the FDTD code is employed to calculate the scattered electric fields that are utilized to mimic the experiments. It should be noted that in the forward problem, the shape function  $F(\theta)$  of the 2-D metallic cylinder buried in a half space is described by the trigonometric series as follows:

$$F(\theta) = \sum_{n=0}^{N/2} B_n \cos(n\theta) + \sum_{n=1}^{N/2} C_n \sin(n\theta) \quad (1)$$

In order to closely describe the shape of the cylinder for both the forward and inverse scattering procedure, the subgridding technique is implemented in the FDTD code, the details are presented in later section.

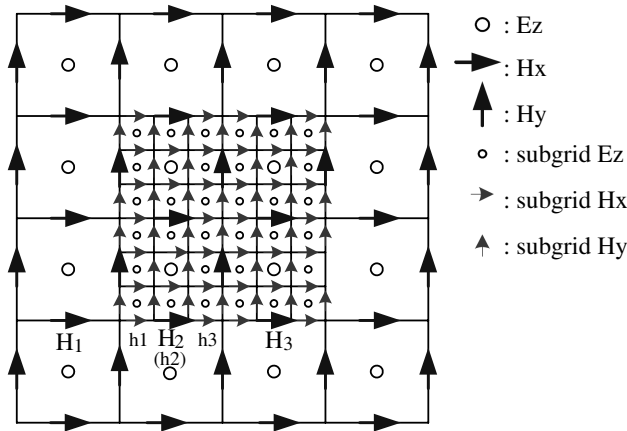


**Figure 2.** Structure of the  $TM_z$  FDTD major grids and local grids for the scaling ratio (1:3),  $H$  fields are aligned with the MG-LG boundary.

A subgridding scheme is employed to divide the problem space into regions of different grid sizes. The grid size in coarse region is about  $(\frac{1}{20} \sim \frac{1}{10} \lambda_{\min})$  as in normal FDTD, while in the fine region the grid size is scaled by an integer ratio. As an example, the Yee cells with subgridding structure are shown in Fig. 2, of which the scaling ratio is 1 : 3.

The capital and small case letters stand for EM fields on the major grids and local grids, respectively. If the scaling ratio is set at odd-ratio then the fields are collocated in space at coarse and fine region. The  $e$  and  $h$  fields inside the fine region can be updated through the normal Yee-cell algorithm except those at the main-grid-local-grid (MG-LG) boundary. The noncollocated magnetic field at the MG-LG interface can be obtained by linearly interpolation. The time interpolation of the fine grid magnetic field at the MG-LG interface is performed using the parabolic interpolation calculation. The above is only a brief introduction to the subgridding FDTD. More detail on

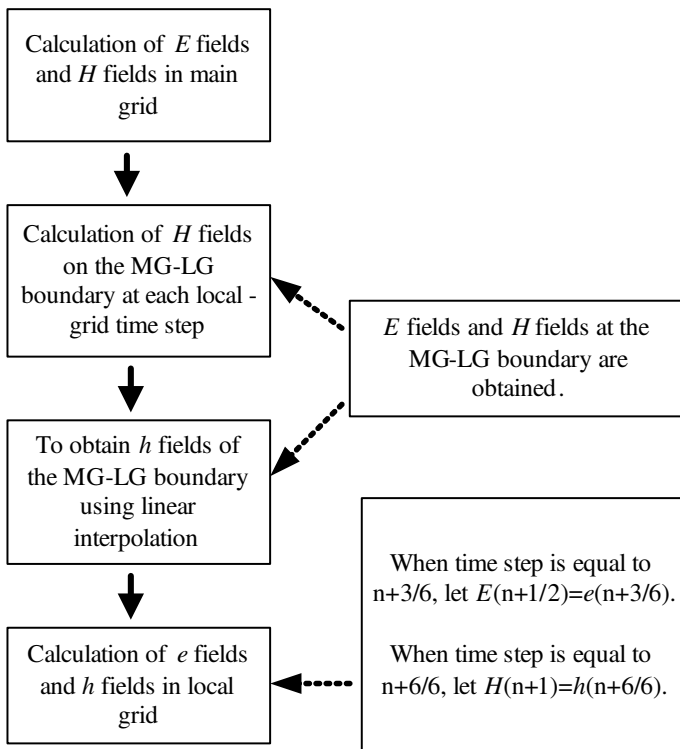


**Figure 3.** Flowchart to update the  $(E, H)$  fields on the major grids and  $(e, h)$  fields on local grids.

subgridding FDTD can be found in [20]. The flow chart associated upon subgrid FDTD computing procedure is shown in Fig. 3.

### 3. INVERSE PROBLEM

For the inverse scattering problem, the shape and location of the metallic cylinder are reconstructed by the given scattered electric field obtained at the receivers. This problem is resolved by an optimization approach, for which the global searching scheme PSO is employed to minimize the following objective function ( $OF$ ):

$$OF = \frac{\sum_{n=1}^{N_i} \sum_{m=1}^M \sum_{q=0}^Q |E_z^{\text{exp}}(n, m, q\Delta t) - E_z^{\text{cal}}(n, m, q\Delta t)|}{\sum_{n=1}^{N_i} \sum_{m=1}^M \sum_{q=0}^Q |E_z^{\text{exp}}(n, m, q\Delta t)|} \quad (2)$$

where  $E_z^{\text{exp}}$  and  $E_z^{\text{cal}}$  are experimental electric fields and the calculated electric fields, respectively. The  $N_i$  and  $M$  are the total number of the transmitters and receivers, respectively.  $Q$  is the total time step number of the recorded electric fields. The details of the proposed PSO are represented as follows.

#### 3.1. Modified Asynchronous Particle Swarm Optimization (APSO)

Particle swarm global optimization is a class of derivative-free, population-based and self-adaptive search optimization technique. Particles (potential solutions) are distributed throughout the searching space and their positions and velocities are modified based on social behavior. The social behavior in PSO is a population of particles moving towards the most promising region of the search space. Clerc [21] proposed the constriction factor to adjust the velocity of the particle for obtaining the better convergence; the algorithm was named as constriction factor method. PSO starts with an initial population of potential solutions that is randomly generated and composed  $N_p$  individuals (also called particles) which represents the location and the geometrical radiuses of the cylinders.

After the initialization step, each particle of population has assigned a randomized velocity and position. Thus, each particle has a position and velocity vector, and moves through the problem space. In each generation, the particle changes its velocity by its best experience, called  $x_{pbest}$ , and that of the best particle in the swarm, called  $x_{gbest}$ .

Assume there are  $N_p$  particles in the swarm that is in a search space in  $D$  dimensions, the position and velocity could be determine according to the following equations (constriction factor method):

$$v_{id}^k = \chi \cdot \left( v_{id}^{k-1} + c_1 \cdot \varphi_1 \cdot (x_{pbest,id} - x_{id}^{k-1}) + c_2 \cdot \varphi_2 \cdot (x_{gbest,id} - x_{id}^{k-1}) \right) \quad (3)$$

$$x_{id}^k = x_{id}^{k-1} + v_{id}^k \quad (4)$$

where  $\chi = \frac{2}{2 - \phi - \sqrt{\phi^2 - 4\phi}}$ ,  $\phi = c_1 + c_2 \geq 4$ .  $c_1$  and  $c_2$  are learning coefficients, used to control the impact of the local and global component in velocity Equation (3).  $v_{id}^k$  and  $x_{id}^k$  are the velocity and position of the  $i$ -th particle in the  $d$ -th dimension at  $k$ -th generation,  $\varphi_1$  and  $\varphi_2$  are both the random number between 0 and 1. It should be mentioned that the  $V_{\max}$  method is also applied to control the particle's searching velocity and to confine the particle within the search space [14]. The "damping boundary condition" proposed by Huang and Mohan [18] to ensure the particles move within the legal search space.

The key distinction between APSO and a typical synchronous PSO is on the population updating mechanism. In the synchronous PSO, the algorithm updates all the particles velocities and positions using Equations (3) and (4) at end of the generation. And then update the best positions,  $x_{pbest}$  and  $x_{gbest}$ . Alternatively, the updating mechanism of APSO is that the new best position is found after each particle position updates if the best position is better than the current best position. The new best position will be used in following particles swarm immediately. The swarm reacts more quickly to speedup the convergence because the updating occurs immediately after objective function evaluation for each particle.

The flowchart of the APSO (APSO) is shown in Fig. 4. APSO goes through seven procedures as follows:

- I. Initialize a starting population: Randomly generate a swarm of particles.
- II. Calculate  $E$  fields by a home-made FDTD code.
- III. Evaluate the population using objective function: The APSO algorithm evaluates the objective function (2) for each individual in the population.
- IV. Find  $x_{pbest}$  and  $x_{gbest}$ .
- V. Mutation scheme: The particle swarm optimization (PSO) algorithm has been shown to converge rapidly during the initial stages of a global search, but when around global optimum, the search can become very slow. For the reason, mutation scheme

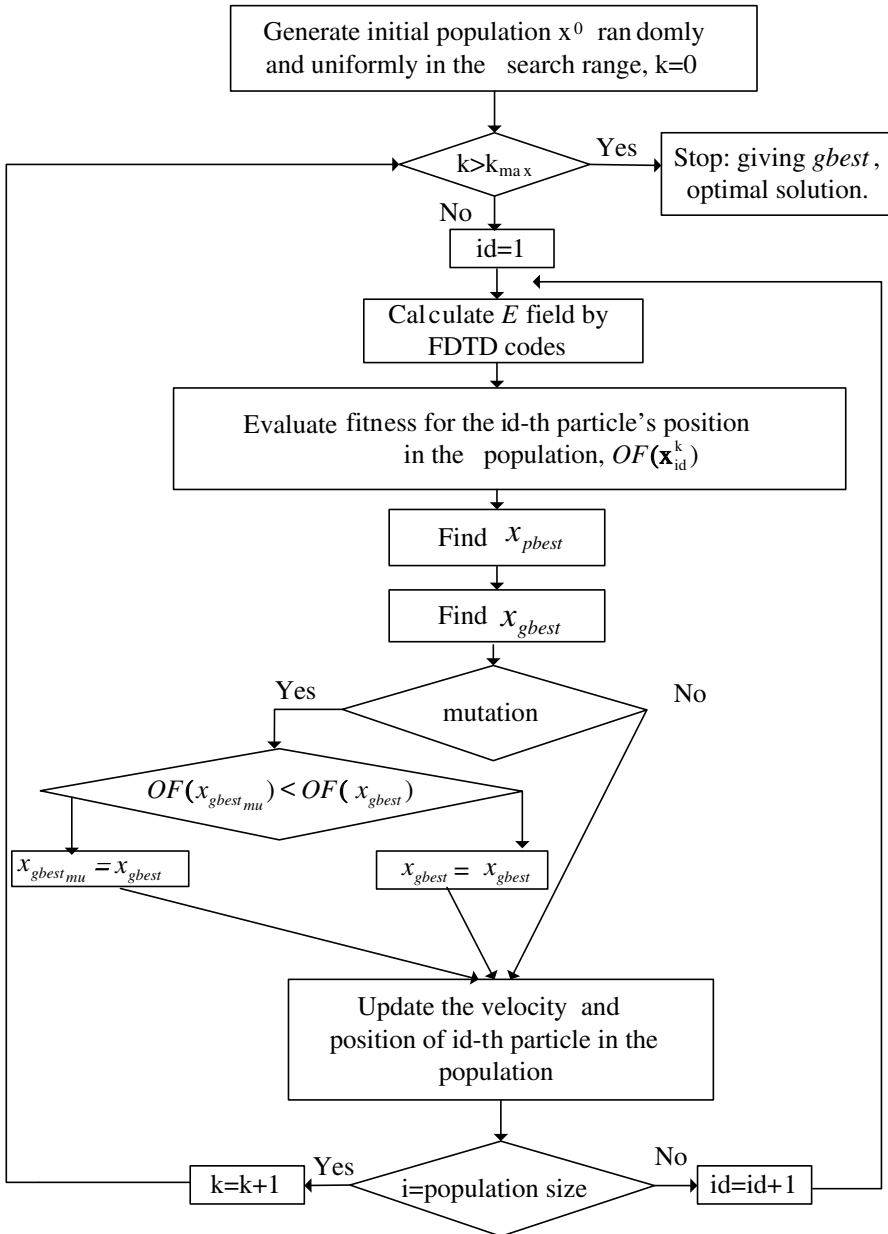


**Figure 4.** Flowchart for the modified APSO.

is introduced in this algorithm to speed up the convergence when particles are around global optimum. The mutation scheme can also avoid premature convergences in searching procedure and help the  $x_{gbest}$  escape from the local optimal position. As shown in Fig. 4, there is an additional competition between the  $x_{gbest}$  and  $x_{pbest_{mu}}$ . The current  $x_{gbest}$  will be replaced by the  $x_{gbest_{mu}}$  if the  $x_{gbest_{mu}}$  is better than the current  $x_{gbest}$ . The  $x_{gbest_{mu}}$  is generated by following way:

$$X_{gbest_{mu}} = \begin{cases} X_{gbest} - \varphi_3 \cdot \left[ c_3 - (c_3 - c_4) \cdot \frac{k}{k_{max}} \right] \cdot (x_{max} - x_{min}), & \text{if } \varphi_{mu} < 0.5 \\ X_{gbest} + \varphi_3 \cdot \left[ c_3 - (c_3 - c_4) \cdot \frac{k}{k_{max}} \right] \cdot (x_{max} - x_{min}), & \text{if } \varphi_{mu} \geq 0.5 \end{cases} \quad (5)$$

where  $c_3$  and  $c_4$  are the scaling parameter.  $\varphi_3$  and  $\varphi_{mu}$  are both the random number between 0 and 1.  $k$  is the current iteration number.  $k_{max}$  is the maximum iteration number.  $x_{max}$  and  $x_{min}$  are the upper limit and lower limit of the search space, respectively.

- VI. Update the velocity and position.
- VII. Stop the process and print the best individual if the termination criterion is satisfied, else go to Step II.

### 3.2. Cubic Spline Interpolation Technique

It should be noted that in the inverse problem, the shape function of the 2-D metallic cylinder is described by a cubic spline in this study instead of the trigonometric series described in the section of the forward problem. The cubic spline is more efficient in terms of the unknown number required to describe a cylinder of arbitrary cross section. By using the cubic spline the coordinates of local origin inside the cylinder serve as the searching parameter and can move around the searching space, which is impossible if the trigonometric series expansion is used in the inversion procedure.

As shown in Fig. 5, the cubic spline consists of the polynomials of degree 3  $P_i(\theta)$ ,  $i = 1, 2, \dots, N$ , which satisfy the following smooth conditions:

$$\begin{aligned} P_i(\theta_i) &= P_{i+1}(\theta_i) \equiv \rho_i \\ P'_i(\theta_i) &= P'_{i+1}(\theta_i) \\ P''_i(\theta_i) &= P''_{i+1}(\theta_i) \end{aligned} \quad i = 1, 2, \dots, N \quad (6)$$

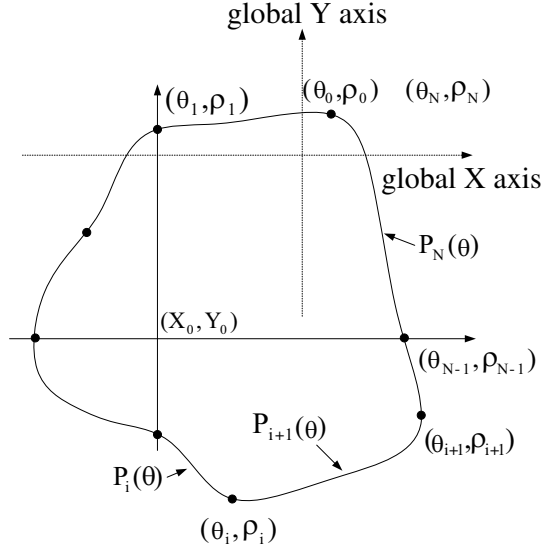


**Figure 5.** Geometry of the cubic-spline.  $(\theta_i, \rho_i)$  is the polarized-coordinate expression for each point and  $P_i(\theta)$  is the function of the cubic line which links the points  $(\theta_{i-1}, \rho_{i-1})$  and  $(\theta_i, \rho_i)$ .

and

$$\begin{aligned}
 P_1(\theta_0) &= P_N(\theta_N) \\
 P'_1(\theta_0) &= P'_N(\theta_N) \equiv \rho'_N \\
 P''_1(\theta_0) &= P''_N(\theta_N)
 \end{aligned} \tag{7}$$

Through the interpolation of the cubic spline, an arbitrary smooth cylinder can be easily described through the radius parameters  $\rho_1, \rho_2, \dots, \rho_N$  and the slope  $\rho'_N$ , of which the details are referred to [19]. By combining the modified APSO and the cubic spline interpolation technique, we are able to reconstruct the microwave image efficiently.

It should be noted that the coordinates of local origin inside the cylinder plus the radiuses of the geometrical spline used to describe the shape of the cylinder will be determined by the APSO scheme.

#### 4. NUMERICAL RESULTS

As shown in Fig. 1, the problem space is divided in  $128 \times 68$  grids with the grid size  $\Delta x = \Delta y = 5.95$  mm. The metallic cylinder is buried in region 2 ( $\sigma_1 = \sigma_2 = \sigma_3 = 0$ ). The transmitters and receivers are placed in region 1. The permittivities in region 1, region 2 and region 3 are

characterized by  $\varepsilon_1 = \varepsilon_0$ ,  $\varepsilon_2 = 8\varepsilon_0$  and  $\varepsilon_3 = \varepsilon_0$ , respectively, while the permeability  $\mu_0$  is used for each region, i.e., only non-magnetic media are concerned here. The cylindrical object is illuminated by a transmitter at two different positions,  $N_i = 2$ , which are located at the  $(-143 \text{ mm}, 178.5 \text{ mm})$  and  $(143 \text{ mm}, 178.5 \text{ mm})$ , respectively. The scattered  $E$  fields for each illumination are collected at the five receivers,  $M = 5$ , which are equally separated by  $47.8 \text{ mm}$  along the distance of  $48 \text{ mm}$  from the half-space interface. The excitation waveform  $I_z(t)$  of the transmitter is the Gaussian pulse, given by:

$$I_z(t) = \begin{cases} Ae^{-\alpha(t-\beta\Delta t)^2}, & t \leq T_w \\ 0, & t > T_w \end{cases} \quad (8)$$

where  $\beta = 24$ ,  $A = 1000 \text{ V/m}$ ,  $\Delta t = 13.337 \text{ ps}$ ,  $T_w = 2\beta\Delta t$ , and  $\alpha = \left(\frac{1}{4\beta\Delta t}\right)^2$ .

The time duration is set to  $300\Delta t$  ( $q = 300$ ). Note that in order to describe the shape of the cylinder more accurately, the subgridding FDTD technique is employed both in the forward scattering (1 : 9) and the inverse scattering (1 : 5) parts — but with different scaling ratios as indicated in the parentheses.

Three examples are investigated for the inverse scattering of the proposed structure by using the modified APSO. There are eleven unknown parameters to retrieve, which include the center position  $(X_O, Y_O)$ , the radius  $\rho_i$ ,  $i = 1, 2, \dots, 8$  of the shape function and the slope  $\rho'_N$ . Very wide searching ranges are used for the modified APSO to optimize the objective function given by (2). The parameters and the corresponding searching ranges are listed follows:  $-47.6 \text{ mm} \leq X_O \leq 47.6 \text{ mm}$ ,  $-47.6 \text{ mm} \leq Y_O \leq 47.6 \text{ mm}$ ,  $5.95 \text{ mm} \leq \rho_i \leq 71.4 \text{ mm}$ ,  $i = 1, 2, \dots, 8$ ,  $-1 \leq \rho'_N \leq 1$ . The operational coefficients for the PSO are set out below. The learning coefficients,  $c_1$  and  $c_2$ , are set to 2, and the population size is set to 30. The relative coefficient of the modified APSO are set as below: The learning coefficients,  $c_1$  and  $c_2$ , are set to 2.8 and 1.3 respectively. The mutation probability is 0.1 and the population size is set to 30 [12].

For the first example, the metallic cylinder with shape function  $F(\theta) = 29.75 - 5.95 \sin(2\theta) \text{ mm}$  is considered. The final reconstructed shape by APSO at the 300th generation is compared to the exact shape in Fig. 6. The final reconstructed shapes by PSO and APSO at the 600th generation are compared to the exact shape in Fig. 7. The discrepancy of shape Function (DF) of the reconstructed shape  $F^{cal}(\theta)$  with respect to the exact values versus generations is shown in Fig. 8. It is shown that the APSO scheme is able to achieve good convergences

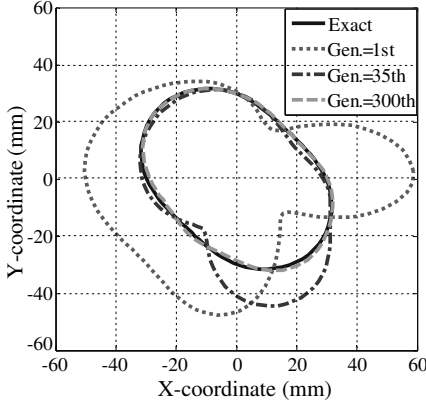


**Figure 6.** The reconstructed shape of the cylinder at different generations for example 1.

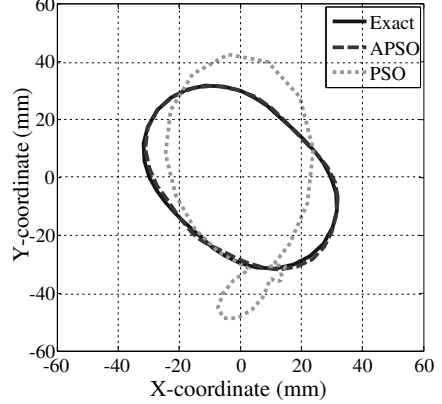


**Figure 7.** The reconstructed shapes of the cylinder for example 1 by PSO and APSO, respectively.

within 200 generations. Here, DF is defined as

$$DF = \left\{ \frac{1}{N'} \sum_{i=1}^{N'} \left[ F^{cal}(\theta_i) - F(\theta_i) \right]^2 / F^2(\theta_i) \right\}^{1/2} \quad (9)$$

where the  $N'$  is set to 720. The r.m.s. error DF for PSO and APSO are about 19.7% and 2.4% in the final generation, respectively. In order to investigate the sensitivity of the imaging algorithm against the random noise, the additive white Gaussian noise of zero mean is added into the experimental electric fields. The relative noise level (RNL) is defined as:

$$RNL = \frac{\sigma_g}{\sqrt{\frac{\sum_{n=1}^{N_i} \sum_{m=1}^{M_i} \sum_{k=0}^K |E_z^{exp}(n, m, k\Delta t)|^2}{(N_i)(M_i)(K-1)}}} \quad (10)$$

The relative noise level of  $10^{-5}$ ,  $10^{-4}$ ,  $10^{-3}$ ,  $10^{-2}$  and 0.1 are used in PSO and APSO for simulation purpose. Fig. 9 shows the reconstructed results under the condition that the experimental scattered field is contaminated by the noise. It could be observed that good reconstruction has been obtained for shape of the metallic cylinder when the relative noise level is below  $10^{-3}$ .

In the second example, the shape function of this object is given by  $F(\theta) = 29.75 + 5.95 \cos(3\theta)$  mm. Fig. 10 shows the final reconstructed shape by APSO at the 300th generation as compared to the exact shape

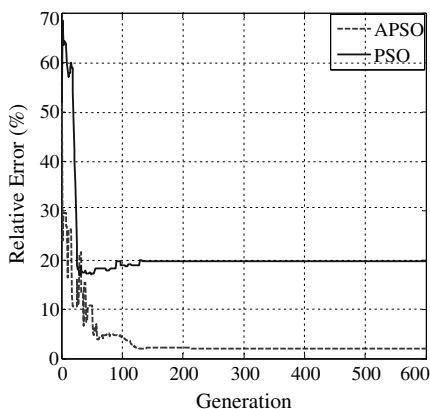


**Figure 8.** Shape function error versus generation for example 1 by PSO and APSO, respectively.

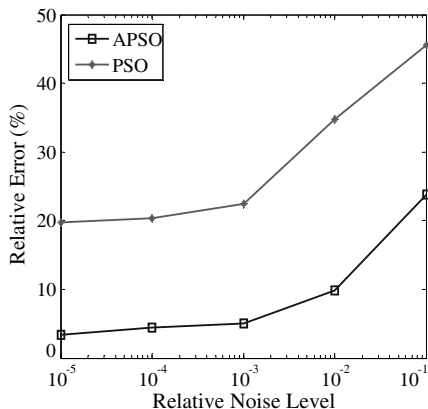


**Figure 9.** Shape error as function of RNL by PSO and APSO, respectively.

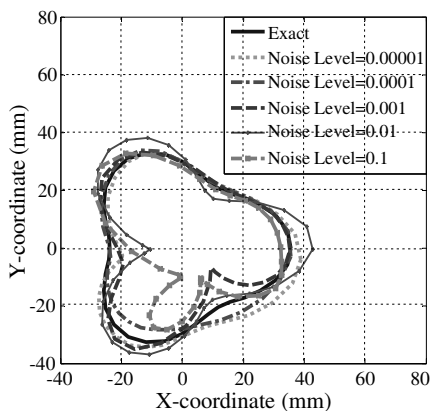


**Figure 10.** The reconstructed shapes of the cylinder under the different RNLs for example 2.

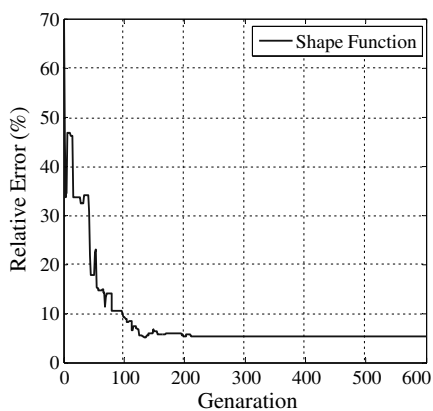


**Figure 11.** Shape function error versus generation for example 2.

in the different levels of RNL. Fig. 11 shows that the relative errors of the shape decrease quickly and good convergences are achieved within 200 generation without noise. The r.m.s. error DF is about 5.53% in the final generation. This example show the imaging quality of the backside of the scatterer is poor due to the shadowing effect.

For the third example, the metallic cylinder with shape function  $F(\theta) = 29.75 + 17.85 \sin(\theta) + 5.95 \cos(3\theta)$  mm is considered. The final

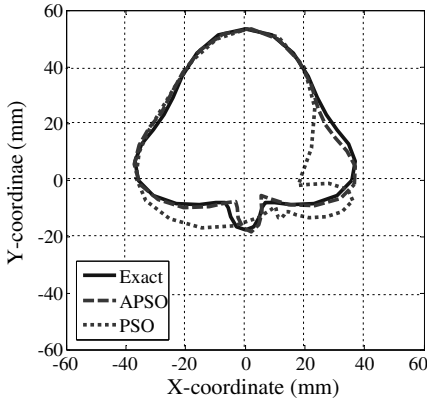


**Figure 12.** The reconstructed shapes of the cylinder at different generations for example 3 by PSO and APSO, respectively.

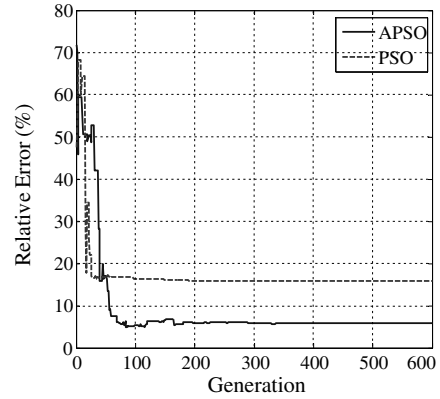


**Figure 13.** Shape function error versus generation for example 3 by PSO and APSO, respectively.

reconstructed shapes by PSO and APSO at the 600th generation are compared to the exact shape in Fig. 12. Fig. 13 shows that APSO the relative errors of the shape decrease quickly and good convergences are achieved within 200 generation. The r.m.s. error DF for PSO and APSO are about 18.3% and 5.7% in the final generation, respectively. From the reconstructed results this object, we conclude the APSO scheme can be used to reconstruct metallic cylinder.

## 5. CONCLUSION

In this paper, we study the time domain inverse scattering of an arbitrary cross section metallic cylinder buried in slab medium. By combining the FDTD method and the APSO, good reconstructed results are obtained. The key differences between PSO [11] and APSO are about the convergence speed, the computation time and the accuracy, since APSO includes “damping boundary condition” scheme and mutation scheme. The inverse problem is reformulated into an optimization one, and then the global searching scheme APSO is employed to search the parameter space. By using the APSO, the shape of the object can be successfully reconstructed. In our study, even when the initial guess is far from the exact one, the APSO can still yield a good solution for the properties of the object. Numerical results have been carried out and good reconstruction has been obtained even in the presence of white Gaussian noise in experimental data.

## REFERENCES

1. Colton, D. and L. Paivarinta, "The uniqueness of a solution to an inverse scattering problem for electromagnetic waves," *Archive for Rational Mechanics and Analysis*, Vol. 119, No. 1, 59–70, Mar. 1992.
2. Tikhonov, A. N. and V. Y. Arsenin, *Solutions of Ill-posed Problems*, Winston, Washington, DC, 1977.
3. Ping, X. W. and T. J. Cui, "The factorized sparse approximate inverse preconditioned conjugate gradient algorithm for finite element analysis of scattering problems," *Progress In Electromagnetics Research*, Vol. 98, 15–31, 2009.
4. Bindu, G., A. Lonappan, V. Thomas, C. K. Aanandan, and K. T. Mathew, "Dielectric studies of corn syrup for applications in microwave breast imaging," *Progress In Electromagnetics Research*, Vol. 59, 175–186, 2006.
5. Chien, W., "Inverse scattering of an un-uniform conductivity scatterer buried in a three-layer structure," *Progress In Electromagnetics Research*, Vol. 82, 1–18, 2008.
6. Bermiani, E., S. Caorsi, and M. Raffetto, "Geometric and dielectric characterization of buried cylinders by using simple time-domain electromagnetic data and neural networks," *Microwave and Optical Technology Letters*, Vol. 24, No. 1, 24–31, Jan. 2000.
7. Moghaddam, M. and W. C. Chew, "Study of some practical issues in inversion with the born iterative method using time-domain data," *IEEE Transactions on Antennas and Propagation*, Vol. 41, No. 2, 177–184, Feb. 1993.
8. Abenius, E. and B. Strand, "Solving inverse electromagnetic problems using FDTD and gradient-based minimization," *International Journal for Numerical Methods in Engineering*, Vol. 68, No. 6, 650–673, Nov. 2006.
9. Rekanos, I. T., "Time-domain inverse scattering using lagrange multipliers: An iterative FDTD-based optimization technique," *Journal of Electromagnetic Waves and Applications*, Vol. 17, No. 2, 271–289, 2003.
10. Chen, X., D. Liang, and K. Huang, "Microwave imaging 3-D buried objects using parallel genetic algorithm combined with FDTD technique," *Journal of Electromagnetic Waves and Applications*, Vol. 20, No. 13, 1761–1774, 2006.
11. Huang, C. H., C. C. Chiu, C. L. Li, and K. C. Chen, "Time domain inverse scattering of a two-dimensional homogenous dielectric object with arbitrary shape by particle swarm optimization,"

- Progress In Electromagnetic Research*, Vol. 82, 381–400, 2008.
12. Carlisle, A. and G. Dozier, “An off-the-shelf PSO,” *Proceedings of the 2001 Workshop on Particle Swarm Optimization*, 1–6, 2001.
  13. Semnani, A. and M. Kamyab, “An enhanced hybrid method for solving inverse scattering problems,” *IEEE Transactions on Magnetics*, Vol. 45, 1534–1537, Mar. 2009.
  14. Zhong, X. M., C Liao, and W. Chen, “Image reconstruction of arbitrary cross section conducting cylinder using UWB pulse,” *Journal of Electromagnetic Waves Application*, Vol. 21, No. 1, 25–34, 2007.
  15. Huang, T. and A. S. Mohan, “A hybrid boundary condition for robust particle swarm optimization,” *IEEE Antennas and Wireless Propagation Letters*, Vol. 4, 112–117, 2005.
  16. Chen, X. and K. Huang, “Microwave imaging of buried inhomogeneous objects using parallel genetic algorithm combined with FDTD method,” *Progress In Electromagnetics Research*, Vol. 53, 283–298, 2005.
  17. Taflov, A. and S. Hagness, *Computational Electrodynamics: The Finite-difference Time-domain Method*, Artech House, Boston, MA, 2000.
  18. Chevalier, M. W., R. J. Luebbers, and V. P. Cable, “FDTD local grid with material traverse,” *IEEE Trans. Antennas and Propagation*, Vol. 45, No. 3, Mar. 1997.
  19. De Boor, C., *A Practical Guide to Splines*, Springer-Verlag, New York, 1978.
  20. Li, C. L., C.-W. Liu, and S.-H. Chen, “Optimization of a PML absorber’s conductivity profile using FDTD,” *Microwave and Optical Technology Lett.*, Vol. 37, 380–383, 2003.
  21. Clerc, M., “The swarm and the queen: Towards a deterministic and adaptive particle swarm optimization,” *Proceedings of Congress on Evolutionary Computation*, 1951–1957, Washington, DC, 1999.